JOURNAL OF SOLID STATE CHEMISTRY 108, 305–313 (1994)

# Bulk and Surface Properties of Copper-Containing Oxides of the General Formula $LaZr_{1-X}Cu_XO_3$

J. A. Anderson and J. L. G. Fierro

*Instituto de Catálisis y Petroleoquimica, C.S.I.S., Campus UAM., Cantoblanco, 28049 Madrid, Spain*

Received January 26, 1993; in revised form June 1, 1993; accepted June 3, 1993

Compounds of nominal composition $LaZr_{1-X}Cu_XO_3$ ($0 \leq X \leq 1$) have been prepared by thermal decomposition in air of precursors prepared by the amorphous citrate method. X-ray diffraction has been used to determine the phases present in the material following calcination at 973 K and following calcination and reduction at 973 K. X-ray photoelectron spectroscopy (XPS) was used to obtain information regarding electronic state and concentration of elements in the surface layers, while thermal gravimetric (TG) studies in hydrogen indicate the relative stability of copper species towards reduction. For all values of $X$ except 1, the pyrochlore phase, $La_2Zr_2O_7$ was obtained. CuO was detected for all values of $X$ greater than 0, whereas $LaCuO_3$ and $La_2CuO_4$ were only detected for values of $X > 0.3$. These phases containing copper were reduced within the temperature range 350–800 K, leading to formation of metallic copper and $La(OH)_3$ and $La_2O_3$. © 1994 Academic Press, Inc.

## INTRODUCTION

Perovskite-type oxides have the general formula $ABO_3$ where the possible range of cations in the $A$ and $B$ positions may be predicted in terms of a tolerance factor by considering the limits of the sizes of the two cations (1). The range of materials of this type may be considerably increased by partial substitution of either the $A$ or $B$ ion by a third cation or of both $A$ and $B$ to produce a substituted perovskite containing four different cations. Partial substitution by a cation of valence less than 3 may lead to the formation of complex oxides while still retaining the perovskite structure. Perovskite materials offer the possibility of relating structure to catalytic activity and selectivity (2). Generally the $A$ cations are catalytically inactive, whereas metal ions in the $B$ position, which are active, may be partially substituted, leading to significant selectivity changes for a given reaction. Previously in this laboratory, copper-containing perovskites of the type $LaM_{1-X}Cu_XO_3$, where $M$ = Mn and Ti, have been prepared and characterized (3, 4), and their activity and selectivity in CO hydrogenation have been tested (5, 6). The present paper outlines the preparation of materials of the general formula $LaZr_{1-X}Cu_XO_3$ and the characterization by XPS, XRD, and TG analysis.

## EXPERIMENTAL

### *Materials*

The amorphous citrate precurors of the materials of nominal composition $LaZr_{1-X}Cu_XO_3$ were prepared according to a previously published method (7). To a concentrated solution of the metal salts in the desired proportion, containing lanthanum nitrate from Fluka, zirconium acetylacetonate from Fluka, and copper acetate from Carlo Erba, a concentrated solution of citric acid (Merck) was added such that the number of gram equilvalents added was the same as the total number of gram equivalents of metal. Due to the limited solubility of copper acetate, nitric acid was added to aid dissolution. The solution was evaporated at 343 K under reduced pressure until a viscous syrup was produced. This material was then dried in air at 383 K to produce a glassy solid, before calcination at the higher temperature. The latter stage involved heating at 5 K $min^{-1}$ to 973 K and then maintaining this temperature for a period of 5 hr. Other materials used in XPS or TG experiments were CuO (Mallinckrodt), $ZrO_2$ (Merck), and $La_2O_3$ which was obtained by thermal decomposition of $La(NO_3)_3 \cdot 6\,H_2O$ (Fluka) at 673 K in air.

### *Methods*

X-ray photoelectron spectra were recorded using a VG ESCALAB 200R spectrometer equipped with a MgK$\alpha$ X-ray source ($h\nu$ = 1253.6 eV) and a hemispherical electron analyzer. Powdered samples were pressed inside small stainless-steel cylinders and outgassed in the pretreatment chamber at $10^{-5}$ torr before transferring into the analysis chamber. Either 20 or 50 (in the case of Cu) eV energy regions of the photoelectrons of interest were scanned at a pass energy of 50 eV, enabling good resolution and reasonable acquisition times. Each spectral region was averaged over a number of scans in order to



0022-4596/94 $6.00
Copyright © 1994 by Academic Press, Inc.
All rights of reproduction in any form reserved.

obtain good signal-to-noise ratios. The carbon 1*s* peak with binding energy of 284.9 eV was used as an internal standard.

Thermogravimetric studies were conducted using a Cahn 2100 RG microbalance, operating at 10 $\mu$g accuracy. Between 30–80 mg of the sample was heated (4 K min$^{-1}$) in a flow (60 cm$^3$ min$^{-1}$) of He up to 673, or 423 K in the case of the CuO reference, and then cooled to approximately 373 K under He. The sample was then heated (4 K min$^{-1}$) in a flow (60 cm$^3$ min$^{-1}$) of $H_2$ to 973 K and weight losses were assumed to be the result of the reduction of oxides of copper.

XRD analysis was performed using a Phillips PW 1716/30 diffractometer using nickel filtered CuK$\alpha$ (0.154 nm) radiation. The diffraction patterns were recorded over the range of 2$\theta$ angles between 5 and 70°, and the *d*-spacings were compared with the ASTM powder files to confirm sample identity.

## RESULTS AND DISCUSSION

### *XRD of Oxidized Samples*

The citrate preparation method is chosen as perovskites are formed at lower temperatures than for processes involing other amorphous precursors. This lower calcination temperature subsequently gives rise to the formation of oxides which display higher BET surface areas (2, 7–9), with the greatest loss in surface area due to sintering being observed in the temperature range 973–1203 K (2). Samples calcined at 773 K exhibited a single broad peak corresponding to a *d*-spacing of ca. 0.3 nm, indicating that the material was still essentially amorphous after such treatment. Diffractograms obtained following a calcination procedure of 5 h at 973 K are shown in Fig. 1. Increasing the calcination time from 5 to 16 h at 973 K did not alter the diffraction pattern, whereas increasing the temperature from 973 to 1073 K resulted in slightly sharper, more defined peaks, indicative of a more ordered, crystalline sample. However, in the interest of obtaining samples with the maximum possible surface areas, 5 h at 973 K was selected as the standard preparation procedure. Peaks labeled Al refer to the aluminum template used to support the samples during analysis. For all samples other than $X = 1$, lanthanum zirconate was present as may have been predicted from the phase diagram of $ZrO_2$-$La_2O_3$ (10), where $La_2Zr_2O_7$ is formed regardless of the proportions of both oxides. For $X = 0$, $La_2Zr_2O_7$ was the only detected phase. The high-temperature stable form of $ZrO_2$ has the fluorite structure, which may be stabilized following cooling to room temperature by the addition of dopant ions such as yttrium or lanthanum (11, 12). These stabilized zirconias contain randomly distributed oxygen vacancies. When an equimolar amount of a suitable trivalent cation (such as $La^{3+}$ here) is added, the pyrochlore structure $A_2B_2O_7$ is formed. This may be regarded as a fluorite structure with an ordered arrangement of oxygen vacancies (13). For all values of $X$ other than 0, copper(II) oxide was detected. This was the only copper-containing phase present for $X = 0.3$, whereas at higher copper substitution, $La_2CuO_4$ and $LaCuO_3$ were present. The synthesis of pure $LaCuO_3$ (14) and mixed $La_2CuO_4$, $LaCuO_3$, CuO phases has been reported during the preparation of $LaMn_{1-X}Cu_XO_3$ (15, 16); however, the $LaCuO_3$ phase was not identified in recent studies using preparation procedures identical to those used here where copper was substituted for *B* cations Mn and Ti (3, 4, 6). It was suggested (3, 4) that the oxygen-deficient structure $LaCuO_{2.5}$ (or $La_2Cu_2O_5$) underwent decomposition under the experimental conditions.

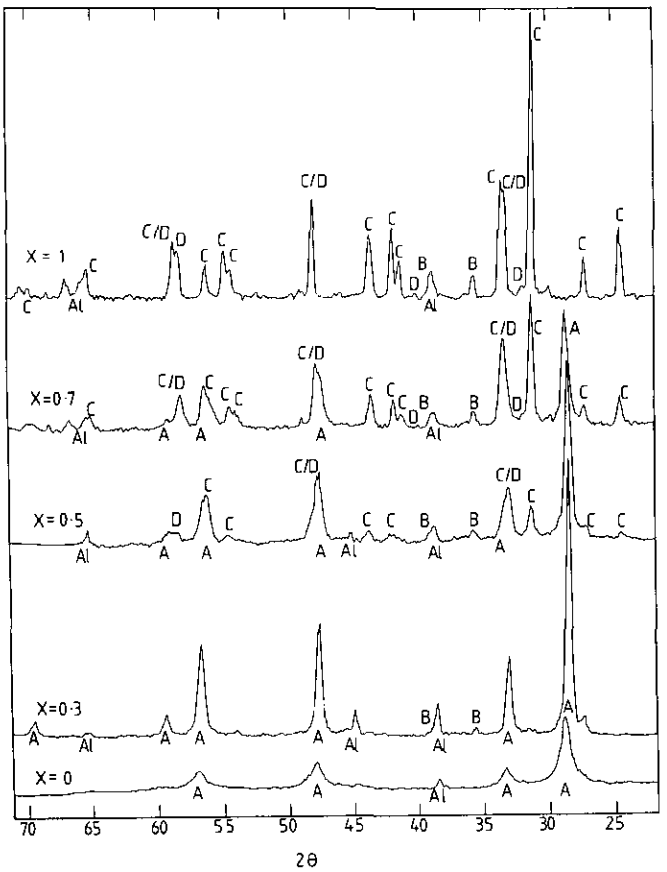


FIG. 1. X-ray diffraction patterns of samples with nominal composition $LaZr_{1-X}Cu_XO_3$ following calcination at 973 K: (A) $La_2Zr_2O_7$, (B) CuO, (C) $La_2CuO_4$, and (D) $LaCuO_3$.

$$La_2Cu_2O_5 \longrightarrow La_2CuO_4 + CuO. \qquad (1)$$

However, this oxide has a tolerance factor (*t*) as defined by $t = r_A + r_O/\sqrt{2}(r_B + r_O)$ of 0.86 (where $r_A$, $r_B$, and $r_O$ are the ionic radii of $La^{3+}$, $Cu^{2+}$, and $O^{2-}$, respectively)

and which lies within the limits of $0.75 < t < 1.0$ which allows for the existence of the perovskite structure. The lack of consistency between these studies may result from the difficulty in distinguishing between the diffraction patterns of $LaCuO_3$ and $La_2CuO_4$. Four of the most intense peaks for $LaCuO_3$ are due to reflections from planes with $d$-spacings of 0.2716, 0.1932, 0.1588, and 0.1581 nm which compare with peaks which appear at 0.2704, 0.1904, 0.1593, and 0.1583 nm in the diffractogram of $La_2CuO_4$ (17). Fortunately, relative intensities (17) of 25 and 45% for the (030) or (300) and (214) planes with $d$-spacings of 0.1588 and 0.1581 nm, respectively, of $LaCuO_3$, and of only 4% for the (133) and (313) reflections from $La_2CuO_4$ planes with $d$-spacings of 0.1593 and 0.1583 nm, assist in identification. Additionally, minor peaks due to the reflections of the 110 and 202 planes (0.2752 and 0.2241 nm) help confirm the assignment. The structure $A_2BO_4$ or $AO(ABO_3)$ is related to the perovskite structure since the $B$ atoms have the same 6-coordinate arrangement of oxygens. However, the $A$ atoms are 9 coordinated to oxygen, whereas they have 12 oxygen neighbors in the perovskite structure. $La_2CuO_4$, which is formed here for values of $X > 0.3$, can be regarded as perovskite sheets, $LaCuO_3$ separated by layers of LaO.

At $X = 0$, no evidence was found for the presence of the perovskite structure $LaZrO_{3+\lambda}$, although the structure falls within the tolerance limits with a value of $t = 0.81$, somewhat less than for the ideal structure with value $t = 1$. It would appear that in order to maintain electroneutrality, the pyrochlore structure $A_2B_2O_7$ is favored against a distorted perovskite structure with an anion excess. Materials of the type $A_2B_2O_7$, in which separate blocks of perovskite-type structure four octahedra thick exist, are known, eg., $Sr_2Ta_2O_7$ (18). Perovskite structures tolerate large oxygen deficiencies better than small oxygen excesses and in this case the excess required for electroneutrality would be rather large.

### *XPS of Oxidized Samples*

The surface of the samples calcined at 973 K was examined by XPS following outgassing in high vacuum, and the appropriate binding energy regions corresponding to O1$s$, La4$d$, Zr3$d$, and Cu2$p$ were recorded. The binding energy values for the series of samples are summarized in Table 1 along with reference compounds $La_2O_3$, $ZrO_2$, and CuO. For the O1$s$ peak, the binding energy for the $La_2O_3$ sample is considerably higher than in any of the other reference materials or in the $LaZr_{1-X}Cu_XO_3$ samples. This may be attributed to the fact that the reference $La_2O_3$ surface is highly hydroxylated (4) with the BE of 533.6 eV representative of oxygen in hydroxyl species. Lower BEs in the other samples are therefore representative of lattice oxygen, $O^{2-}$. Despite the presence of several copper phases as detected by XRD, BEs of the Cu2$p_{3/2}$ were essentially identical in all samples and in the reference CuO. Spectra (Fig. 2) show the peaks due to Cu2$p_{3/2}$ and 2$p_{1/2}$ core levels, along with the shake-up satellite peaks at higher binding energies which are characteristic of $Cu^{2+}$ ions. In contrast to the behavior of copper, zirconium, although present in only one phase detectable by XRD, shows significant differences in the nature of the surface Zr species as detected by XPS. For

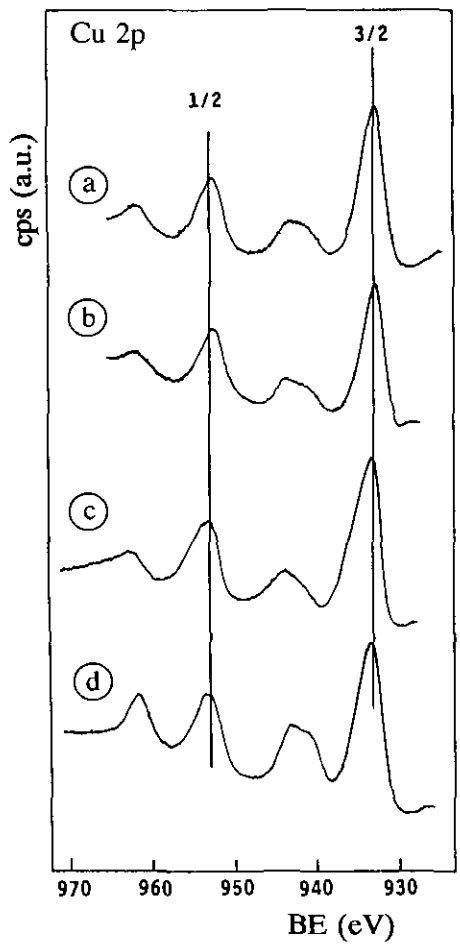


FIG. 2. XP spectra of Cu2$p$ in samples $LaZr_{1-X}Cu_XO_3$ for values of $X$: (a) 0.3, (b) 0.5, (c) 0.7, and (d) 1.0.

TABLE 1
Binding Energies (eV) of Core Electrons in $LaCu_XZr_{1-X}O_\delta$

| Sample | O1$s$ | La4$d_{5/2}$ | Zr3$d_{5/2}$ | Cu2$p_{3/2}$ |
|---|---|---|---|---|
| LaZr | 529.5 | 102.2 | 181.5 | — |
| $Cu_{0.3}Zr_{0.7}$ | 529.0 | 101.5 | 181.0 | 933.0 |
| $Cu_{0.5}Zr_{0.5}$ | 528.7 | 101.3 | 179.6 | 932.8 |
| $Cu_{0.7}Zr_{0.3}$ | 529.1 | 101.5 | 180.8 | 933.3 |
| LaCu | 528.7 | 101.7 | — | 933.4 |
| $La_2O_3$ | 533.6 | 101.5 | — | — |
| $ZrO_2$ | 529.7 | — | 181.6 | — |
| CuO | 528.7 | — | — | 932.8 |

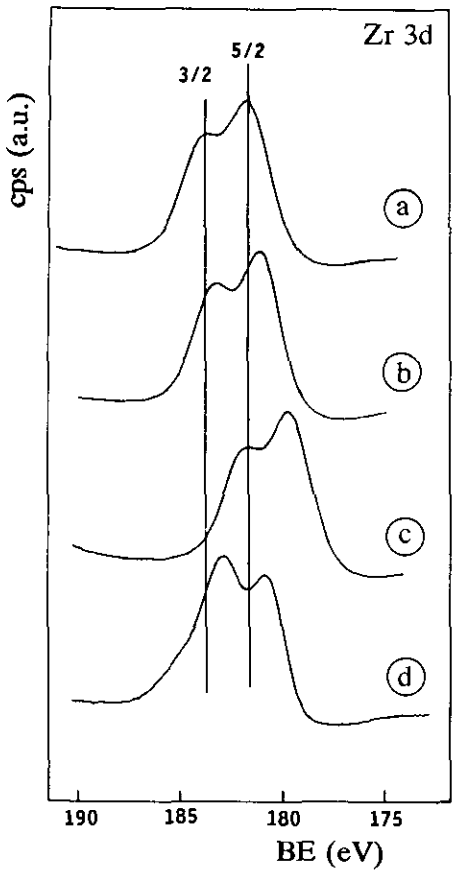


FIG. 3. XP spectra of Zr3$d$ in samples $LaZr_{1-X}Cu_XO_3$ for values of $X$: (a) 0, (b) 0.3, (c) 0.5, and (d) 0.7.

TABLE 2
Surface XPS Intensity Ratios of $LaCu_XZr_{1-X}O_\delta$ Samples

| Sample | Cu/(La + Zr) | Zr(La + Zr) | C[a]/La |
|---|---|---|---|
| LaZr | 0.000 | 0.479 | 0.22 |
| $Cu_{0.3}Zr_{0.7}$ | 0.092 | 0.334 | 0.18 |
| $Cu_{0.5}Zr_{0.5}$ | 0.088 | 0.319 | 0.13 |
| $Cu_{0.7}Zr_{0.3}$ | 0.148 | 0.254 | 0.13 |
| LaCu | 0.132 | 0.000 | 0.43 |
| $La_2O_3$ | — | — | 0.30 |

[a] Atomic ratios of carbonate C1$s$/total La4$d$.

the sample where $X = 0$, where equimolar amounts of Zr and La would favor the formation of a single pyrochlore structure (13), the Zr3$d_{5/2}$ binding energy is essentially identical to that in the reference $ZrO_2$ (Table 1). Decreasing the Zr/La ratio by increasing $X$ from 0 to 0.5 decreases the Zr3$d_{5/2}$ binding energy (Table 1) which, from Fig. 3, can be seen as a progressive shift of the Zr3$d$ doublet. However, at $X = 0.7$, the progressive shift is interrupted and the 3$d_{5/2}$ peak (Table 1) appears between those in the samples of $X = 0.3$ and 0.5. Additionally, analysis of the 3$d$ doublet (Fig. 3) reveals a change in the relative intensities of the 3/2 and 5/2 peaks, and a pronounced tailing to the higher BE side of the former. These two characteristics may be interpreted by considering the spectrum as composed of signals from two distinct zirconium species. To determine whether this may be related to an enrichment (or depletion) or zirconium from the surface of this particular sample, the XPS intensity ratios were calculated (Table 2). When plotted against the nominal sample composition (Fig. 4), it is observed that for each sample, the surface Zr concentration as sampled by XPS correlates almost exactly with the bulk concentration. Although the value for $X = 0.7$ lies marginally above the line of exact surface/nominal correlation in contrast to all other samples, this is not considered significant. The identification of two distinct Zr surface species for sample $X = 0.7$ is attributed to the presence of a Zr–O type species and to a hydroxide- or carbonate- (see below) type entity.

The presence of more than one type of surface species was also apparent for La, where XP spectra, particularly for $X = 0.7$ and $X = 1$, clearly show deviation from the expected doublet (Fig. 5). In all cases, the spectra could be accurately deconvoluted by assuming the presence of two types of species (two doublets). In addition to the major component due to the oxide, giving the binding energies listed in Table 1, a nonoxide-type species gives rise to a signal at higher binding energies. This would be consistent with the presence of hydroxide- or carbonate-type species. The presence of the latter was confirmed in the range of the carbon 1$s$ signal where a signal at ca. 289 eV, indicative of carbon oxygen bonding in carbonate structures, was found. However, the calculated atomic

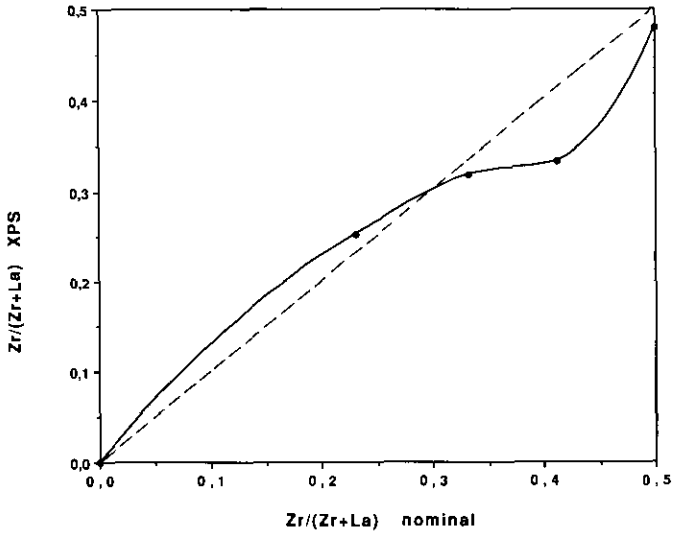


FIG. 4. Relationship between surface Zr intensity ratios as measured by XPS and nominal bulk Zr content.

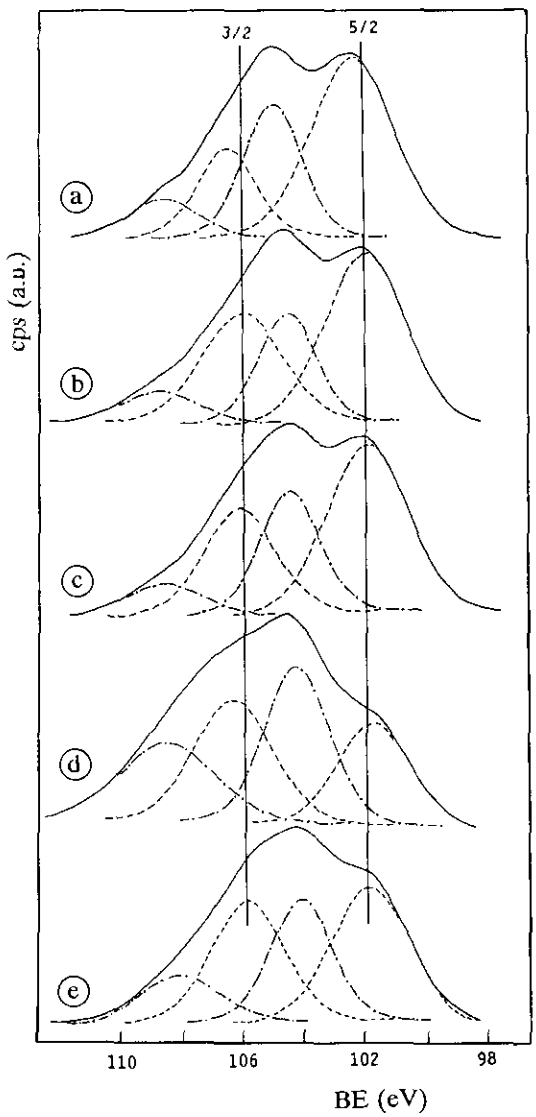


FIG. 5. XP spectra of La4*d* in samples $LaZr_{1-X}Cu_XO_3$ for values of $X$: (a) 0, (b) 0.3, (c) 0.5, (d) 0.7, and (e) 1.0 show contributions due to oxide species (---) and nonoxide species (- · - · -).

ratios of this signal to the signal for the nonoxide type La species ranged from 0.25 ($X$ = 0.7) to 1.2 ($X$ = 1.0), indicating that a single common species (i.e., carbonate) is not the sole contributor to the nonoxide La signal. A mixture of carbonate, hydroxide, and hydroxycarbonate species is probably present. Using the high BE peak of the C1*s* and total area of the La4*d* peaks, the relative proportions of carbonate species in each sample were calculated. The results suggest (Table 2), that carbonate is present in relatively lower concentrations in the presence of Zr than in its absence. This is attributed to the relative basicity of the surfaces, with La in the presence of Zr forming the relatively weakly basic $La_2Zr_2O_7$ phase, and La in its absence, where the phases $La_2CuO_4$ an $La_2O_3$ are favored, exhibiting high basicity and hence strongly adsorbing $CO_2$.

In contrast with the correlation between Zr surface and nominal compositions, surface XPS intensity ratios calculated for copper (Table 2) indicate low detected levels when compared with the nominal bulk content (Fig. 6). This would suggest the presence of particulate phases containing copper, eg., CuO. The observation that the surface Cu signal does not vary appreciably with an increase in nominal copper content would suggest that on increasing the Cu concentration, larger particulate phases of copper (e.g., CuO) are formed.

*Thermogravimetric Analysis*

The thermograms (mg lost per gram of starting material) in hydrogen as a function of temperature are shown in Fig. 7 for the samples and reference CuO. Reduction of bulk copper oxide was initiated at 450 K and completed by 475 K in agreement with previous experiments conducted in this laboratory (3, 4). The derivative of the weight loss/temperature profile shows maxima at 462 and 468 K, the latter in close agreement with results of van der Grift *et al.* (19), but at somewhat lower temperatures than maximum reported by other workers (20, 21). The presence of two maxima in the derivative plot may be attributed to reduction of Cu(II) and Cu(I) oxides as a result of reduction of CuO to Cu via $Cu_2O$ (20–22) as observed for high loaded supported Cu catalysts (21). As shown by Himelfarb *et al.* (22), $Cu^0$ was not formed until all CuO was reduced to $Cu_2O$, thus explaining the presence of two resolvable maxima here. For all samples in the series $LaZr_{1-X}Cu_XO_3$, except $X$ = 0.3, some reduction was observed below the onset reduction temperature of

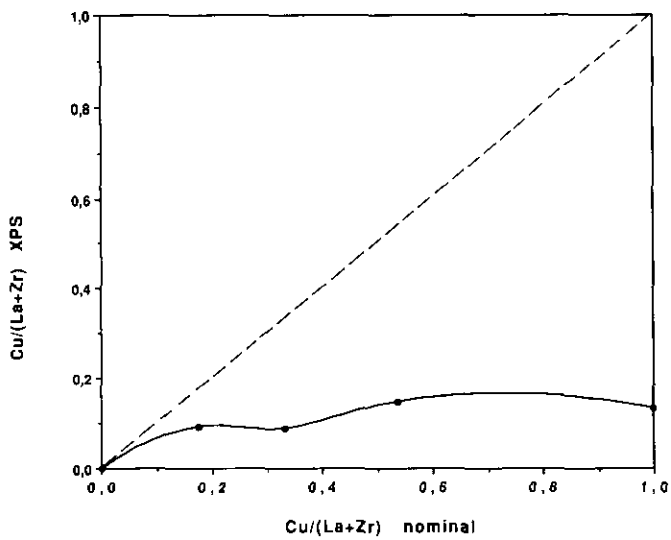


FIG. 6. Relationship between surface Cu intensity ratios as measured by XPS and nominal bulk Cu content.

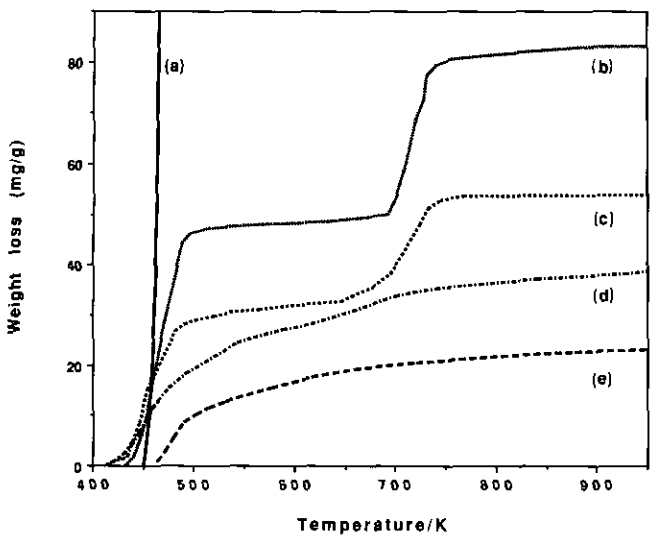


FIG. 7. Thermograms of reference CuO (a), and samples with nominal composition $LaZr_{1-X}Cu_XO_3$ with values of $X$; (b) 1.0, (c) 0.7, (d) 0.5, and (e) 0.3.

bulk CuO, consistent with reports that supported CuO is reduced below the temperature of reduction of the bulk oxide (19–21) due to the larger reductive surface area and the number of defects at which the reduction process may be initiated. For the samples $X = 0.7$ and 1.0, a reduction step between 650 and 750 K is consistent with those in studies of $LaTi_{1-X}Cu_XO_3$ (3) and $LaMn_{1-X}Cu_XO_3$ (4) for $X = 1$, where this step was attributed to reduction of $La_2CuO_4$.

$$La_2CuO_4 + H_2 \longrightarrow La_2O_3 + Cu + H_2O. \quad (2)$$

The generation of water during this reduction would lead either to surface hydroxylation or to the formation of bulk hydroxide, $La(OH)_3$ (see following section). A reduction stage with a maximum rate at ca. 700 K in the sample $X = 0.5$ was not clearly discernible despite the detection of the $La_2CuO_4$ phase by XRD. A maximum of two clear reduction stages was observed for materials $LaTi_{1-X}Cu_XO_3$ (3) and $LaMn_{1-X}Cu_XO_3$ (4) only in the case of the sample with $X = 1$. However, other substitution values led to complex reduction profiles due to the presence of three reducible copper-containing phases, although the reduction steps were not clearly resolved. Similarly, here three clear reduction stages were not observed for any of the samples despite the detection of three copper phases by XRD. Samples $X = 0.3$ and 0.5 show an initial weight loss below 500 K, indicating reduction of CuO, the only copper-containing phase identified by XRD for sample $X = 0.3$. Above 500 K there is a gradual but continual weight loss. Unlike the thermograms of samples $X = 1$ and 0.7, the temperature range between 500 and 600 K was not marked by an absence in weight loss for the lower substituted samples. This may indicate the slow reduction of other copper-containing phases, as detected by XRD for the $X = 0.5$ sample, or the decomposition/hydrogenation of other species not removed during the pretreatment in He. Weight losses of 23.4, 39.9, 56.3, and 83.0 mg/g compare with theoretical values of 17.5, 30.2, 41.3, and 63.9, mg/g for reduction of copper in the samples where $X = 0.3$ to 1, clearly indicating the presence of an additional source of weight loss in hydrogen. Attempts to remove such species by the use of higher temperature pretreatments led to further complications. When samples were pretreated in flowing He up to 973 instead of 673 K, the subsequent weight losses in $H_2$ were less than the theoretical values for complete reduction of copper in the samples. Also, the sample weight loss below 500 K appeared to show a correlation with the period of time for which the sample was left at 973 K in He. This would suggest a degree of decomposition of copper oxide in He at this temperature, and would be consistent with XPS results of other copper-containing mixed oxides (3, 4) where degassing at 723 K resulted in elimination of the shake-up satellite peaks, characteristic of $Cu^{2+}$, from the spectra. However, this need not implicate $Cu^0$, since the ligand $\rightarrow 3d$ charge transfer responsible for such satellites would also be inoperative for $Cu^+$, which also contains completely filled $d$-shells. Outgassing or heating in inert atmosphere above 723 K may not result in complete decomposition of CuO to Cu (3, 4) but may lead to the formation of $Cu_2O$. Additional weight losses in $H_2$ above the theoretical amounts for samples heated in He up to 673 K would suggest the presence of a stable surface species which decomposed or was reduced in $H_2$ at temperatures above 650 K.

In this respect, DRIFTS spectra of samples outgassed at 673 K exhibit an intense doublet with maxima at 1467 and 1395 $cm^{-1}$ (Fig. 8). This doublet is characteristic of carbonate species, and shows a greater degree of correlation with the spectrum of carbonate species on $La_2O_3$ or $La(OH)_3$ (1500, 1390 $cm^{-1}$) (23) and the spectrum of bulk $La_2(CO_3)_3 \cdot 8H_2O$ (1460, 1360 $cm^{-1}$) (24) than carbonate species on $ZrO_2$ (25). Additionally, species derived from $CO_2$ adsorbed on $ZrO_2$ are readily decomposed to $CO_2$ and CO in flowing He in the temperature range 393–453 K (26) in contrast with the behavior of lanthanum carbonate species, which are stable to outgassing up to 973 K (23). These bands cannot be assigned to incompletely decomposed precursor citrate, as previous infrared studies clearly show the elimination of bands due to these species following calcination in air at 573 K (27). Therefore weight losses in $H_2$ above the theoretical values for samples pretreated in He up to 773 K are attributed to decomposition or hydrogenation of surface carbonate species which are ligated to exposed $La^{3+}$ cations. In agreement with the

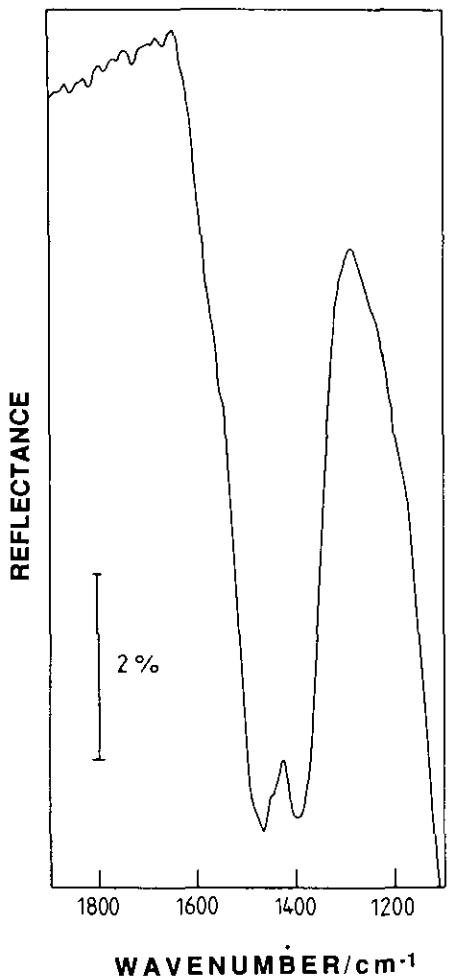


FIG. 8. DRIFT spectrum of $LaZr_{0.5}Cu_{0.5}O_3$ after *in situ* degassing at 673 K (1 hr).

results from XPS analysis, which showed carbonate species to be more abundant for samples in the absence of Zr, sample $X = 1$ displayed the greatest excess weight loss above the theoretical value calculated for the reduction of copper oxides.

In contrast with a previous report for copper-containing mixed oxides (6), samples following reduction at either 773 or 993 K in hydrogen exhibited color changes to black from the brown of the calcined samples, and for the reduced sample $X = 1$, no reddish tinge (6) was observed.

### *XRD of Reduced Samples*

XRD profiles of samples reduced (from TG experiments) at 973 K are shown in Fig. 9, along with identification of phases present. Samples reduced at 773 K showed the presence of the same phases for each sample, although the relative intensities and peak widths did not correlate exactly. Additionally, for samples reduced at 773 K, as for those at 973 K, no traces of oxidized copper phases were identified, confirming that in the TG experiments, weight losses between 650–750 K represent the highest reduction temperature of copper-containing species, and that no unreduced copper species exist beyond this temperature. Copper metal (111 and 200 reflections) were observed for each sample (except $X = 0$), with peak intensities increasing with an increase in the value of $X$. All samples other than $X = 1$ showed the $La_2ZrO_7$ phase, which was the only oxide phase detected in the cases of $X = 0.3$. $La_2O_3$ appears in the diffraction pattern of samples $X = 0.5$, 0.7, and 1, while $La(OH)_3$ was detected only for the latter. The presence of $La_2O_3$, $La(OH)_3$, and Cu phases for reduced samples compares with previous results (3, 4) for mixed oxides of nominal composition $LaCuO_3$. Similarly, $La_2O_3$, but not $La(OH)_3$, was detected for lower substitutions of Cu. This may be attributed to the quantity of water produced during reduction: this being greatest for the highest Cu : La ratio. Complete hydration to the trihydrate may be expected for $La_2O_3$ samples exposed to moisture over a longer period of time, being transformed via LaOOH (3, 4, 28).

Copper crystallite sizes were determined by XRD line broadening from the FWHM of the Cu(111) line in the XRD profiles of the samples reduced at both 773 and 973

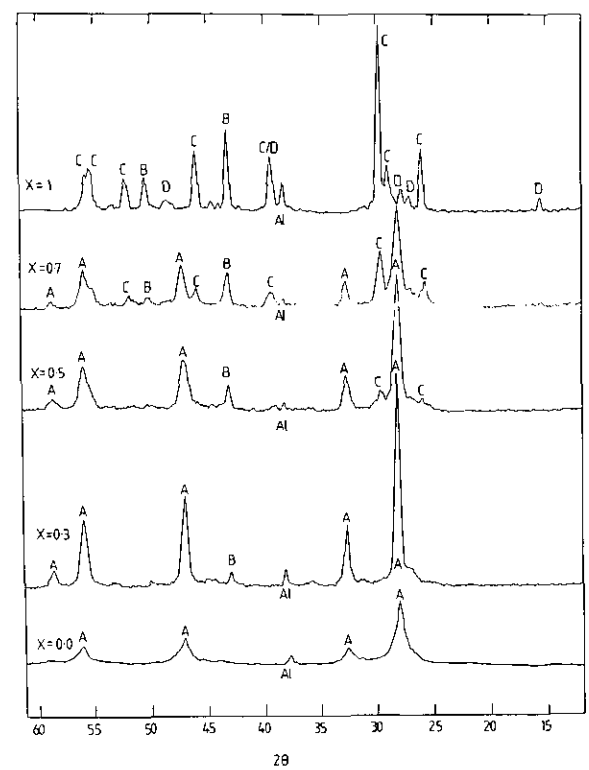


FIG. 9. X-ray diffraction patterns of samples with nominal composition $LaZr_{1-X}Cu_XO_3$ following reduction at 973 K: (A) $La_2Zr_2O_7$, (B) Cu, (C) $La_2O_3$, and (D) $La(OH)_3$.

TABLE 3
Surface Areas and Copper Particle Size in Reduced Samples

| $LaCu_XZr_{1-X}O_\delta$ | $T_{RED}$ 773 K | $T_{RED}$ 973 K | Surface area |
|---|---|---|---|
| $X$ | $d$(nm) | $d$(nm) | ($m^2g^{-1}$) |
| 1.0 | — | 32 | 1.3 |
| 0.7 | 30 | 30 | 2.6 |
| 0.5 | 17 | 30 | 2.0 |
| 0.3 | 30 | 32 | 1.3 |
| 0.0 | — | — | 0.9 |

K (Table 3). Unlike results for $LaTi_{1-X}Cu_XO_3$ (3) and $LaMn_{1-X}Cu_XO_3$ (4), the $d$ values for $Cu^0$ show no strong dependence on the copper content of the sample. For substitution, $X = 1$ in $LaMn_{1-X}Cu_XO_3$, Rojas *et al.* (4) obtained a copper particle of $d = 80$ nm after sample reduction at 973 K, and attributed this large particle size, relative to lower substitutions, to the absence of the perovskite phase. The detection of a significantly smaller particle size obtained in this study reduced under similar conditions may conversely be attributed to the presence of the $LaCuO_3$ perovskite phase, thereby stabilizing the copper in this phase against sintering during high temperature reduction. Increasing the reduction temperature from 773 to 973 K did not have a significant effect on the dispersion except in the case of $X = 0.5$, where the higher reduction temperature favored the formation of a larger copper particle size

*Surface Area Measurement*

The surface areas of the calcined materials as measured by $N_2$ adsorption at 77 K for samples degassed at 413 K are shown in Table 3. Measured areas were low, with a general trend of increasing area with an increase in the value of $X$: the exception being for $X = 1$, where the pyrochlore phase is absent. The presence of this phase may be partly responsible for the lower areas obtained by replacing Cu with Zr rather than Mn (4, 6). However, for complete substitution, this cannot be responsible for differences here and in previous studies (4, 6). One possibility is that low surface areas were the result of the highly exothermic one-step decomposition due to the oxidation of the citrate chains at 553 –573 K as observed in previous studies involving Cu containing precursors (27). Such uncontrolled ignition of samples may also explain differences in the phases detected here and elsewhere (3, 4) for the $X = 1$ samples. Heating in $N_2$ beyond this temperature followed by heating in air to the required calcination temperature may overcome this problem, whereas heating directly to the upper calcination temperature in $N_2$ resulted in heavily carbonized samples which exhibited low surface areas (9). However, in contrast, Bell and co-workers, using two sets of identically prepared precursors, inexplicably obtained identical surface areas for materials calcined at 973 K in air (4) and He (6).

## CONCLUSIONS

Compounds of general formula $LaZr_{1-X}Cu_XO_3$ do not incorporate Zr into a perovskite structure, but favor the formation of the pyrochlore, $La_2ZrO_7$. For the fully substituted compound, $LaCuO_3$ was detected, in contrast with previous observations, indicating that the exact conditions regarding formation of this phase are very select. This phase was not reduced in a stage readily distinguishable from the reduction of the other Cu-containing phases, $La_2CuO_4$ and CuO. TGA, XPS, and IR analysis indicate the surfaces of all samples to be partially covered with a carbonate species, although the proportion covered by this was high only in the absence of zirconium, where basic lanthanum oxides were present.

## ACKNOWLEDGMENTS

We thank Dr. M. L. Rojas for her help in the preparation of these materials and for helpful discussions. Thanks to Prof. C. H. Rochester for access to the DRIFT facility. J. A. A. is grateful to the Royal Society of London for a grant received under the European Science exchange programme.

## REFERENCES

1. V. M. Goldschmidt, *Skr. Nor. Vidensk. Akad., Kl. I: Mat. Naturvidensk Kl.*, 8 (1926).
2. L. G. Tejuca, J. L. G. Fierro, and J. M. D. Tascon, *Adv. Catal.* **36,** 237 (1989).
3. M. L. Rojas and J. L. G. Fierro, *J. Solid State Chem.* **89,** 299 (1990).
4. M. L. Rojas, J. L. G. Fierro, L. G. Tejuca, and A. T. Bell, *J. Catal.* **124,** 41 (1990).
5. R.van Grieken, J. L. Peña, A. Lucas, G. Calleja, M. L. Rojas, and J. L. G. Fierro, *Catal. Lett.* **8,** 335 (1991).
6. J. A. Brown-Bourzutschky, N. Homs, and A. T. Bell, *J. Catal.* **124,** 52 (1990).
7. J. M. D. Tascon, S. Mendioroz, and L. G. Tejuca, *Z. Phys. Chem. N.F.* **124,** 109 (1981).
8. L. Wachowski, *Surf. Coat. Technol.* **29,** 303 (1986).
9. J. I. Di Cosimo, A. J. Marchi, and C. R. Apesteguia, *J. Catal.*, **134,** 594 (1992).
10. G. Smith, Ed., "Phase Diagrams for Ceramists," Vol. 4. The American Ceramic Soc., Columbus, OH, 1981.
11. P. Turlier, J. A. Dalmon, G. A. Martin, and P. Vergon, *Appl. Catal.* **29,** 305 (1987).
12. R. Franklin, P. Goulding, J. Haviland, R. W. Joyner, I. McAlpine, P. Moles, C. Norman, and T. Nowell, *Catal. Today*, **10,** 405 (1991).
13. P. J. Gellings and H. J. M. Bouwmeester, *Catal. Today* **12,** 1 (1992).
14. G. Demazeau, G. Parent, M. Pouchard, and P. Hagenmuller, *Mater. Res. Bull.* **7,** 913 (1972).
15. P. K. Gallagher, D. W. Johnson, Jr., and E. M. Vogel, *J. Am. Ceram. Soc.* **60,** 28 (1977).

16. E. M. Vogel, D. W. Johnson, Jr. and P. K. Gallagher, *J. Am. Ceram. Soc.* **60,** 31 (1977).
17. "ASTM Powder Diffraction Files." Joint Committee on Powder Diffraction Standards, Pennsylvania, 1979.
18. D. M. Smyth, *Ann. Rev. Mater. Sci.* **15,** 329 (1985).
19. C. J. G. van der Grift, A. Mulder, and J. W. Geus, *Appl. Catal.* **60,** 181 (1990).
20. T. H. Fleisch and R. L. Mieville, *J. Catal.* **90,** 165 (1984).
21. J. M. Dumas, C. Geron, A. Kribii, and J. Barbier, *Appl. Catal.* **47,** L-9 (1989).
22. P. B. Himelfarb, F. E. Wawner, Jr., A. Bieser, Jr., and S. N. Vines, *J. Catal.* **83,** 469 (1983).
23. M. P. Rosynek and D. T. Magnuson, *J. Catal.* **48,** 417 (1977).
24. P. E. Caro, J. O. Sawyer, and L. Eyring, *Spectrochim. Acta, Part A* **28,** 1167 (1972).
25. N. E. Tret'yakov, D. V. Pozdnyakov, O. M. Oranskaya, and V. N. Filimonov, *Russ. J. Phys. Chem. Engl. Transl.* **44,** 596 (1970).
26. M-Y. He and J. G. Ekerdt, *J. Catal.* **87,** 238 (1984).
27. J. I. Di Cosimo and C. R. Apesteguia, *J. Catal.* **116,** 71 (1989).
28. M. P. Rosynek and D. T. Magnuson, *J. Catal.* **46,** 402 (1977).